Eur. Phys. J. C (2020) 80:1091
https://doi.org/10.1140/epjc/s10052-020-08534-2

THE EUROPEAN PHYSICAL JOURNAL C

Regular Article - Experimental Physics

Sensitivity to neutrinos from the solar CNO cycle in Borexino

BOREXINO Collaboration[a]

M. Agostini[1], K. Altenmüller[1], S. Appel[1], V. Atroshchenko[2], Z. Bagdasarian[3,d], D. Basilico[4], G. Bellini[4], J. Benziger[5], R. Biondi[6], D. Bravo[4,e], B. Caccianiga[4], F. Calaprice[7], A. Caminata[8], P. Cavalcante[9,f], A. Chepurnov[10], D. D'Angelo[4], S. Davini[8], A. Derbin[11], A. Di Giacinto[6], V. Di Marcello[6], X. F. Ding[7,b], A. Di Ludovico[7], L. Di Noto[8], I. Drachnev[11], A. Formozov[4,12], D. Franco[13], C. Galbiati[7,14], C. Ghiano[6], M. Giammarchi[4], A. Goretti[7,f], A. S. Göttel[3,15], M. Gromov[10,12], D. Guffanti[16], Aldo Ianni[6], Andrea Ianni[7], A. Jany[17], D. Jeschke[1], V. Kobychev[18], G. Korga[19], S. Kumaran[3,15], M. Laubenstein[6], E. Litvinovich[2,20], P. Lombardi[4], I. Lomskaya[11], L. Ludhova[3,15], G. Lukyanchenko[2], L. Lukyanchenko[2], I. Machulin[2,20], J. Martyn[16], E. Meroni[4], M. Meyer[21], L. Miramonti[4], M. Misiaszek[17], V. Muratova[11], B. Neumair[1], M. Nieslony[16], R. Nugmanov[2,20], L. Oberauer[1], V. Orekhov[2], F. Ortica[22], M. Pallavicini[8], L. Papp[1], Ö. Penek[3,15], L. Pietrofaccia[7], N. Pilipenko[11], A. Pocar[23], G. Raikov[2], M. T. Ranalli[6], G. Ranucci[4,c], A. Razeto[6], A. Re[4], M. Redchuk[3,15], A. Romani[22], N. Rossi[6], S. Schönert[1], D. Semenov[11], G. Settanta[3], M. Skorokhvatov[2,20], O. Smirnov[12], A. Sotnikov[12], Y. Suvorov[2,6,g], R. Tartaglia[6], G. Testera[8], J. Thurn[21], E. Unzhakov[11], F. L. Villante[6,24], A. Vishneva[12], R. B. Vogelaar[9], F. von Feilitzsch[1], M. Wojcik[17], M. Wurm[16], S. Zavatarelli[8], K. Zuber[21], G. Zuzel[17]

[1] Physik-Department and Excellence Cluster Universe, Technische Universität München, 85748 Garching, Germany
[2] National Research Centre Kurchatov Institute, 123182 Moscow, Russia
[3] Institut für Kernphysik, Forschungszentrum Jülich, 52425 Jülich, Germany
[4] Dipartimento di Fisica, Università degli Studi and INFN, 20133 Milan, Italy
[5] Chemical Engineering Department, Princeton University, Princeton, NJ 08544, USA
[6] INFN Laboratori Nazionali del Gran Sasso, 67010 Assergi, AQ, Italy
[7] Physics Department, Princeton University, Princeton, NJ 08544, USA
[8] Dipartimento di Fisica, Università degli Studi and INFN, 16146 Genoa, Italy
[9] Physics Department, Virginia Polytechnic Institute and State University, Blacksburg, VA 24061, USA
[10] Lomonosov Moscow State University Skobeltsyn Institute of Nuclear Physics, 119234 Moscow, Russia
[11] St. Petersburg Nuclear Physics Institute NRC Kurchatov Institute, 188350 Gatchina, Russia
[12] Joint Institute for Nuclear Research, 141980 Dubna, Russia
[13] AstroParticule et Cosmologie, Université Paris Diderot, CNRS/IN2P3, CEA/IRFU, Observatoire de Paris, Sorbonne Paris Cité, 75205 Paris Cedex 13, France
[14] Gran Sasso Science Institute, 67100 L'Aquila, Italy
[15] III. Physikalisches Institut B, RWTH Aachen University, 52062 Aachen, Germany
[16] Institute of Physics and Excellence Cluster PRISMA$^+$, Johannes Gutenberg-Universität Mainz, 55099 Mainz, Germany
[17] M. Smoluchowski Institute of Physics, Jagiellonian University, 30348 Kraków, Poland
[18] Institute for Nuclear Research, 03028 Kyiv, Ukraine
[19] Department of Physics, School of Engineering, Physical and Mathematical Sciences, Royal Holloway, University of London, Egham, UK
[20] National Research Nuclear University MEPhI (Moscow Engineering Physics Institute), 115409 Moscow, Russia
[21] Department of Physics, Technische Universität Dresden, 01062 Dresden, Germany
[22] Dipartimento di Chimica, Biologia e Biotecnologie, Università degli Studi e INFN, 06123 Perugia, Italy
[23] Amherst Center for Fundamental Interactions and Physics Department, University of Massachusetts, Amherst, MA 01003, USA
[24] Dipartimento di Scienze Fisiche e Chimiche, Università dell'Aquila, 67100 L'Aquila, Italy

Received: 26 May 2020 / Accepted: 12 October 2020 / Published online: 26 November 2020

[a] e-mail: spokesperson-borex@lngs.infn.it
[b] e-mail: xuefengd@princeton.edu
[c] e-mail: gioacchino.ranucci@mi.infn.it (corresponding author)
[d] Present address: Department of Physics, University of California, Berkeley, 94720 Berkeley, CA, USA
[e] Present address: Departamento de Física Teórica, Universidad Autónoma de Madrid, Campus Universitario de Cantoblanco, 28049 Madrid, Spain

Abstract Neutrinos emitted in the carbon, nitrogen, oxygen (CNO) fusion cycle in the Sun are a sub-dominant, yet crucial component of solar neutrinos whose flux has not been measured yet. The Borexino experiment at the Laboratori Nazionali del Gran Sasso (Italy) has a unique opportunity to detect them directly thanks to the detector's radiopurity and the precise understanding of the detector backgrounds. We discuss the sensitivity of Borexino to CNO neutrinos, which is based on the strategies we adopted to constrain the rates of the two most relevant background sources, *pep* neutrinos from the solar *pp*-chain and ^{210}Bi beta decays originating in the intrinsic contamination of the liquid scintillator with ^{210}Pb. Assuming the CNO flux predicted by the high-metallicity Standard Solar Model and an exposure of 1000 days $\times$ 71.3 t, Borexino has a median sensitivity to CNO neutrino higher than 3 σ. With the same hypothesis the expected experimental uncertainty on the CNO neutrino flux is 23%, provided the uncertainty on the independent estimate of the ^{210}Bi interaction rate is 1.5 cpd/100 ton. Finally, we evaluated the expected uncertainty of the C and N abundances and the expected discrimination significance between the high and low metallicity Standard Solar Models (HZ and LZ) with future more precise measurement of the CNO solar neutrino flux.

1 Introduction

The Sun releases energy mainly through a nuclear fusion process known as the proton–proton chain (*pp* chain). Another process, called the carbon–nitrogen–oxygen (CNO) cycle (see Fig. 1), is expected to contribute about one percent of the total energy and neutrino production [1,2]. The CNO cycle emits neutrinos with energies up to around 1.2 MeV and 1.7 MeV for its two main components, see Fig. 2. This process, thought to be the dominant energy production process for stars heavier than 1.3 solar masses [3] as well as solar-like stars in advanced evolutionary stages [4], has many implications for astrophysical problems. For example, the measurement of CNO neutrinos would allow the evaluation of the efficiency of the CNO cycle, helping with the determination of the age of globular clusters [5]. It would also provide a direct reading of the metal abundance in the solar core, which would in turn allow the study of the chemical evolution paradigm assumed by the standard solar model (SSM) [6].

Currently the CNO neutrino rate is only measured to be less than 8.1 counts per day per 100 ton (hereinafter as cpd/100 ton) at 95% confidence level by Borexino [7]. This paper presents a detailed study of the sensitivity of the Borexino experiment to CNO neutrinos. The study relies on a precise and independent determination of the two main residual background components: ^{210}Bi contamination of the liquid scintillator, which can be estimated using measurements of ^{210}Po decays (as suggested in [8]), and *pep* solar neutrinos, which are a part of the *pp* chain.

After a brief overview of the Borexino detector in Sects. 2, 3 discusses Borexino's sensitivity to CNO neutrinos. Section 4 present the strategy to constrain the backgrounds and the influence of additional purification of the liquid scintillator. In Sect. 5 we comment on the relevance of the measurement of the flux of CNO neutrinos in the context of solar physics, with an emphasis on the "solar metallicity (or abundance) problem". This scientific puzzle originated when a re-determination of the surface metallicity of the Sun [9–13] indicated a lower value than previously assumed [14]. However, solar models incorporating these lower metal abundances [10] meet difficulties in reproducing the results from helioseismology, which support models with a higher metal content. Section 5.1 shows that, by following the approach

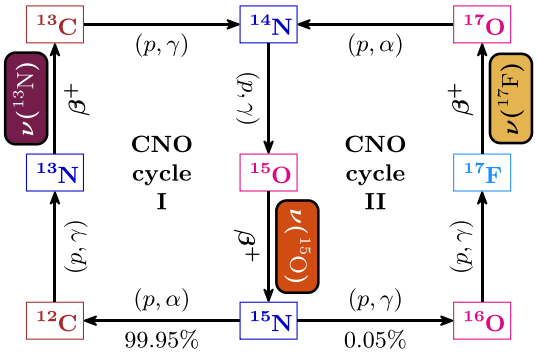

Fig. 1 Two branches (CNO-I and CNO-II) of the CNO cycle of proton–proton fusion to ^{4}He. Only the former is complete in the Sun's core [2]

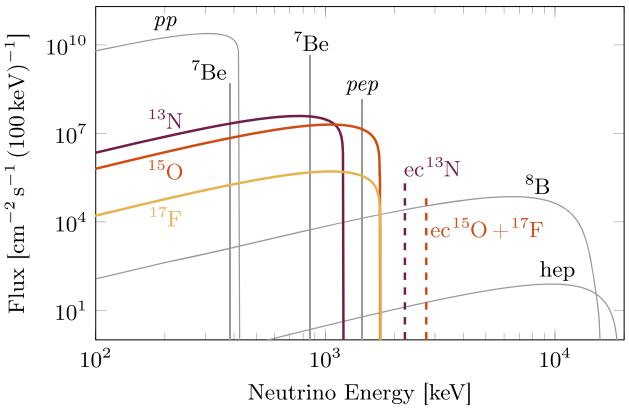

Fig. 2 Solar neutrino spectra predicted by the *B16 (GS98)-HZ* Standard Solar Model [6]. For monochromatic lines, the vertical axis reports the flux in cm^{-2} s^{-1}. The so-called ^{13}N and ^{15}O neutrinos are produced by the β^+-decays of Nitrogen-13 and Oxygen-15 in the CNO-I-branch of the CNO-cycle, respectively. The Fluorine-17 component is essentially negligible in the Sun

[f] Present address: INFN Laboratori Nazionali del Gran Sasso, 67010 Assergi, AQ, Italy

[g] Present address: Dipartimento di Fisica, Università degli Studi Federico II e INFN, 80126 Naples, Italy

proposed in [15,16], it is possible to infer the carbon and nitrogen contents of the solar core independently of the assumed opacity of solar plasma by combining a CNO neutrino flux measurement with the very precise measurement of the ^{8}B neutrino flux by the Super-Kamiokande collaboration [17] (about 2% precision). Finally, Sect. 5.2 discusses the possibility of using a CNO neutrino measurement to discriminate among SSMs with different hypotheses about the Sun's surface metallicity by combining a measurement of the CNO neutrino flux with existing ^{7}Be and ^{8}B data measured by Borexino [7].

2 The Borexino experiment

The Borexino detector [20] has been taking data since 2007 in the Laboratori Nazionali del Gran Sasso (Italy) at a depth of 3800 m.w.e. Borexino is an unsegmented calorimeter using about 280 ton of ultra-pure organic liquid scintillator. The scintillator consists of PC (pseudocumene, 1,2,4-trimethyl-benzene) as a solvent with 1.5 g/l of fluor PPO (2,5-diphenyloxazole) as a solute. The electron density is $(3.307 \pm 0.015) \times 10^{31}$ e$^-$ per 100 ton. This scintillator is contained in a 125 μm-thick nylon vessel with a nominal radius of 4.25 m. It is surrounded by non-scintillating buffer fluid contained in a 6.85 m radius stainless steel sphere, which supports 2212 8-in. ETL 9351 photomultipliers (PMTs). The stainless steel sphere is submerged in ultra-pure water serving as an active muon veto and a passive shield against external radiation.

Neutrinos are detected via the elastic scattering reaction on electrons in the liquid scintillator. The electrons deposit their energy in the scintillator, which results in scintillation light. To measure this deposited energy, several energy estimators are developed [18,19] and they give consistent results in solar neutrino analyses. In this work, we use the variable N_h, the overall number of hits on the PMTs, as a baseline. The interaction vertex is reconstructed via the arrival times of the scintillation photons on the PMTs. As a reference, the detected photoelectron yield is ∼500 photoelectrons/MeV (normalized to 2000 PMTs). The energy and position reconstruction uncertainties at 1 MeV are ∼ 50 keV and ∼ 10 cm, respectively.

The time distribution of the detected hits on the PMTs allows pulse-shape discrimination (PSD). With PSD, α particles, a product of ^{210}Po decay in the scintillator, can be discriminated from β particles on an event-by-event basis [21,22]. It can also be used to constrain the ratio of the total counts of β^+ events, such as ^{11}C decays, to β^- events in specific energy ranges [18,19].

3 Borexino sensitivity to CNO neutrinos

In the Borexino Phase-II analysis [7], the signal and background rates were determined using the multivariate fit method. In detail, as discussed in [18,19], we started from a background model consisting of a list of unstable isotopes contaminating the scintillator (namely ^{14}C, ^{85}Kr, ^{210}Po, ^{210}Bi), isotopes of cosmogenic origin (^{11}C), and γ-rays emitted in the regions outside of the sensitive volume and referred to as external backgrounds (originating from decays from ^{208}Tl, ^{214}Bi, and ^{40}K).

We then performed a multivariate fit procedure of events selected in an optimized wall-less fiducial volume (FV) of about 70 ton in the central part of the detector that included two observables: the energy spectra of the events in the region from 0.19 to 2.93 MeV and their reconstructed radial coordinate distribution [19]. This fitting procedure made it possible to disentangle the rates of events induced by neutrinos from those induced by backgrounds. At the same time, the fair goodness-of-fit (p value of 0.7) verified the consistency of the background model.

In this study, we make assumptions of background rates and signal rates based on the multivariate fit analyses of Phase-III data, which starts from 2016 June. The expected energy distribution of the signals and of the most relevant background components can be seen in Fig. 3, while the expected and measured interaction rates of solar neutrinos (Phase-II results) are listed in Table 1, and the expected signal and background rates considered in the present study are listed in Table 2.

There is an intrinsic difficulty in the measurement of solar neutrinos due to the similarity of the energy spectra of ^{210}Bi electrons and those of electron recoils induced by *pep* and CNO neutrinos. This feature, which was discussed in [18,19], is clearly visible in Fig. 3. The partial degeneracy of these spectral shapes induces significant correlations among these three components. Only by constraining the rates of two out of three components can one measure the rate of the third precisely.

However, the measurement of R_{CNO} (i.e., the interaction rate of CNO solar neutrinos) is now possible in Borexino Phase-III as we have identified a strategy (discussed in Sect. 4) to measure or constrain the two main components, *pep* neutrinos and ^{210}Bi in the scintillator. The thermal stabilization of the detector, achieved during the Phase-III period, is fundamental to measure the rate of ^{210}Bi. The low internal background levels, great depth of LNGS, passive detector shielding, and active removal (based on the three-fold-coincidence method [18], i.e. TFC cut) of the cosmogenic ^{11}C background are also crucial.

Further, we observed an energy region from about 0.8 MeV to 1 MeV, hereinafter referred to as region of interest (ROI), that is dominated by R_{Bi}, R_{pep}, and R_{CNO} (see Fig. 4). More precisely, in this ROI the background contributions are of the same order as the statistical fluctuations of the total expected CNO rate. Thus, it is also possible to extract the sensitivity of Borexino to CNO neutrinos through

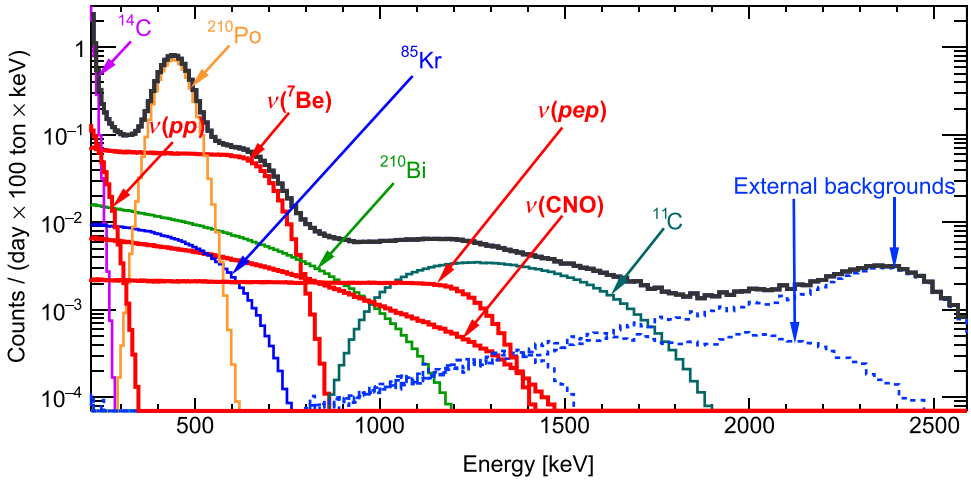

Fig. 3 Expected event energy distribution of an arbitrary exposure without statistical fluctuations and after the fiducial volume cut. The solar neutrino components are highlighted with bold red lines. The spectra of the relevant background contributions are scaled to existing measurements. The contribution of the decay of the ^{11}C isotope reported in the plot is reduced by the application of the three fold coincidence (TFC) procedure described in [18,19]

a simple procedure consisting only of determining the background rates and subsequently counting all the events in this energy region. Section 3.1 first discusses this counting analysis. Then, Sect. 3.2 presents a sensitivity study performed with the multivariate spectral fit. Finally, Sect. 3.3 and 3.4 compare the resulting expected sensitivities and discovery significance from both methods.

In the following sections, our best estimates of the conditions of the Borexino Phase-III are applied. The ^{210}Bi rate R_{Bi} is assumed to be 10 cpd/100 ton. The exposure of 1000 day × 70 ton considers the same fiducial volume as the one applied in the previous solar analysis [7] and amounts to 192 year × ton in total. In the counting analysis, only events after the TFC cut are used, and the exposure loss is 36%. In the multivariate fit analysis, all events are used. In order to facilitate the comparison of the performances of the two methods, we use the same values of the constraint of the *pep* neutrino interaction rates as well as the ^{210}Bi contamination of the scintillator. The *pep* constraint (Sect. 4.1) is based on the predictions of the Standard Solar Model, while ^{210}Bi constraint (Sect. 4.2) is centered in the range considered achievable in Borexino.

We note, that with a high exposure, the intrinsic small difference between the spectral shapes of CNO and ^{210}Bi makes it possible, in principle, to measure the interaction rate of CNO neutrinos without any constraint on R_{Bi}. With a spectral analysis similar to that discussed in this paper, we estimate that the statistical significance of about 3σ can be reached for an exposure of 450 year × ton assuming CNO neutrinos from the HZ SSM. The statistical sensitivity of such analysis improves as the inverse square root of exposure. However, the systematic uncertainties due to the detector response and energy scale modeling must be treated carefully.

Table 1 Expected integral interaction rates (without energy threshold), and corresponding Borexino Phase-II results [7], in cpd/100 ton. The prediction assumes the Standard Solar Model [6] under the high (HZ) and low (LZ) metallicity hypotheses and the MSW-LMA paradigm with the oscillation parameters reported in [23]. The data have been obtained with a total exposure of 1291.51 day×71.3 ton. The CNO interaction rate was constrained to the expected HZ or LZ values in the fit procedure thereby allowing the measurement of the *pp*, ^{7}Be, and *pep* interaction rates. As reported in the table, the interaction rate of *pep* was the only fit component affected by the difference in the CNO values. The upper limit on the CNO neutrino interaction rate was obtained with the fit procedure by constraining the ratio of the *pp* and *pep* rates, with a Gaussian pull-term, to the values predicted by the SSM

Solar ν	B16(GS98)-HZ cpd/100 ton	B16(AGSS09)-LZ cpd/100 ton	Borexino results cpd/100 ton
pp	131.1 ± 1.4	132.2 ± 1.4	$134 \pm 10^{+6}_{-10}$
^{7}Be	47.9 ± 2.8	43.7 ± 2.5	$48.3 \pm 1.1^{+0.4}_{-0.7}$
pep	2.74 ± 0.04	2.78 ± 0.04	$2.43 \pm 0.36^{+0.15}_{-0.22}$(HZ)
			$2.65 \pm 0.36^{+0.15}_{-0.24}$ (LZ)
CNO	4.92 ± 0.78	3.52 ± 0.52	< 8.1 (95% C.L.)

3.1 Borexino as a *counting experiment*

This approach consists of counting the total number of events in the ROI to obtain the interaction rate of CNO neutrinos as the difference between the total number of events detected in ROI and that of the backgrounds, as evaluated in an independent way.

Our key assumptions lie in the availability of a realistic background model and the ability to measure the rate of the residual background components independently (or to label them as negligible). Another assumption is the availability of

Table 2 Assumed rates without energy threshold, expected number of events in the ROI after TFC cut, and fraction of events in the ROI (i.e. ε in Eq. (1)) of each component. The assumed precision of rates of each background is also provided, except that the uncertainty of CNO is calculated from Eq. (2). The efficiencies are estimated using an *ab initio* simulation software [24]. The uncertainties of efficiencies are all less than 0.06%, mainly coming from the uncertainty of the energy scale, so they are neglected. The exposure used here is after TFC cut and is 447 day × 100 ton

Component	Rates cpd/100 ton	Events (N^{ROI})	Efficiencies (ε) %
Total		697 ± 26	
CNO ν	4.92 ± 1.50	162 ± 49	7.37
^{210}Bi	10 ± 2	203 ± 41	4.55
pep ν	2.74 ± 0.04	195.8 ± 2.9	15.98
^{7}Be ν	47.9 ± 1.3	61.2 ± 1.7	0.29
^{11}C	1.5 ± 0.3	32.9 ± 6.6	4.91
ext ^{214}Bi	4 ± 0.6	19.1 ± 2.7	1.07
ext ^{208}Tl	5 ± 0.3	14.47 ± 0.84	0.65
ext ^{40}K	1 ± 0.7	6.4 ± 4.6	1.42
^{85}Kr	12 ± 1.4	1.23 ± 0.14	0.02
^{210}Po	50 ± 2.3	0.06 ± 0.01	0.00

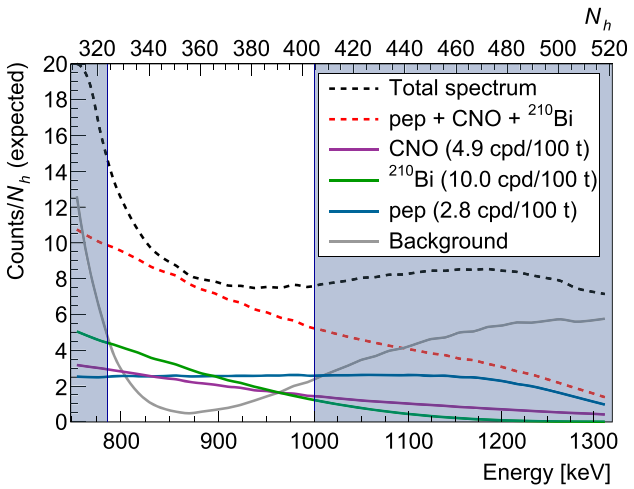

Fig. 4 Expected Borexino event energy distribution of *pep* (solid blue line), CNO neutrino (solid purple line), and ^{210}Bi backgrounds (solid green line) in the region of interest (ROI) used in the counting analysis. The sum of three components is shown as the dashed red line. Other backgrounds are marked as the solid gray line, and the total sum is shown as the black dashed line. The assumed rates are listed in Table 2. As in Fig. 3, events are selected with the fiducial volume cut and the contribution of ^{11}C is suppressed using the TFC procedure. The white region indicates the region of interest

a sufficiently accurate model of the detector response function, needed to determine the fraction of each spectral component in the ROI.

As shown in Figs. 3 and 4, there are six contributions to the event rate in the ROI: CNO neutrinos, ^{210}Bi electrons, *pep* neutrinos, residual ^{11}C positrons, ^{7}Be neutrinos, and external gamma backgrounds. The impact of the relevant parameters like the exposure, the choice of the ROI, and the precision of the estimation of *pep* neutrino and ^{210}Bi rates can be understood by writing R_{CNO} and its statistical uncertainty $\sigma_{\mathrm{CNO}}^{count}$ as:

$$R_{\mathrm{CNO}} = \frac{1}{\varepsilon_{\mathrm{CNO}}}\left(r_{\mathrm{tot}} - \varepsilon_{\mathrm{Bi}}\tilde{R}_{\mathrm{Bi}} - \varepsilon_{pep}\tilde{R}_{pep} - \tilde{r}_{\mathrm{o}}\right) \quad (1)$$

$$\sigma_{\mathrm{CNO}}^{count} = \frac{1}{\varepsilon_{\mathrm{CNO}}}\left(\sigma_{\mathrm{tot}} \oplus \varepsilon_{\mathrm{Bi}}\tilde{\sigma}_{\mathrm{Bi}} \oplus \varepsilon_{pep}\tilde{\sigma}_{pep} \oplus \tilde{\sigma}_{\mathrm{o}}\right) \quad (2)$$

$$r_x = \frac{N_x^{\mathrm{ROI}}}{\mathcal{E}} \ (x = \mathrm{tot}, \mathrm{o})$$

$$\sigma_{\mathrm{tot}} = \frac{\sqrt{N_{\mathrm{tot}}^{\mathrm{ROI}}}}{\mathcal{E}}$$

$$\sigma_{\mathrm{o}} = \varepsilon_{\mathrm{Be}}\tilde{\sigma}_{\mathrm{Be}} \oplus \varepsilon_{\mathrm{C}}\tilde{\sigma}_{\mathrm{C}} \oplus \varepsilon_{\mathrm{ext\,Bi}}\tilde{\sigma}_{\mathrm{ext\,Bi}} \oplus \cdots, \quad (3)$$

where N_x^{ROI} (x =tot(al) or o(thers)) is the number of events in ROI of x, $\mathcal{E}$ is the exposure, ε is the fraction of events for each component falling inside the ROI, R and σ are the rate and the uncertainty, respectively, of components in the full energy range, and r_{o} is the total event rate of all other components in the ROI. The contributions to r_{o} are either negligible and/or independently determined. The ^{7}Be solar neutrino rate is constrained to Phase-II results [7]. ^{85}Kr is determined with the fast coincidence tagging of its minor branch [7]. ^{11}C, external ^{214}Bi, ^{208}Tl, and ^{40}K are determined together with events outside the ROI via the spectral fitting method. ^{210}Po is negligible in the ROI. Variables with a tilde mark the values from independent determinations and the subscripts indicate the spectral component. The symbol $\oplus$ is defined as $a \oplus b = \sqrt{a^2 + b^2}$.

The values of the assumed rates, uncertainties, and efficiencies are listed in Table 2. The ratios of the four terms in Eq. (1), from left to right, are 10:3:3:2. When $\tilde{\sigma}_{\mathrm{Bi}}$ is 1.5 cpd/100 ton and $\tilde{\sigma}_{pep}$ is $1.4\% \cdot \tilde{R}_{pep}$, or 0.04 cpd/100 ton, the ratios of the four terms in Eq. (2), from left to right, are 9:11:1:3. The largest contribution to $\sigma_{\mathrm{CNO}}^{count}$ in Eq. (2) is the ^{210}Bi term unless the uncertainty on the ^{210}Bi constraint is lower than 1.3 cpd/100 ton when $\sigma_{\mathrm{tot}} = \varepsilon_{\mathrm{Bi}}\tilde{R}_{\mathrm{Bi}}$, in which case $\sigma_{\mathrm{CNO}}^{count}$ is limited by a statistical error. The resulting uncertainty on the CNO neutrino interaction rate as a function $\tilde{\sigma}_{\mathrm{Bi}}$ and $\tilde{\sigma}_{pep}$ can be seen in Fig. 5.

3.2 Multivariate fit analysis

We performed a study of the sensitivity of Borexino to CNO neutrinos by simulating tens of thousands of pseudo-experiments and fitting the pseudo-data with the full multivariate procedure as the one used for real data [7]. This approach requires maximizing a two dimensional likelihood function built using two observables (energy estimator and radial position). We assumed, as throughout Sect. 3, that R_{pep}

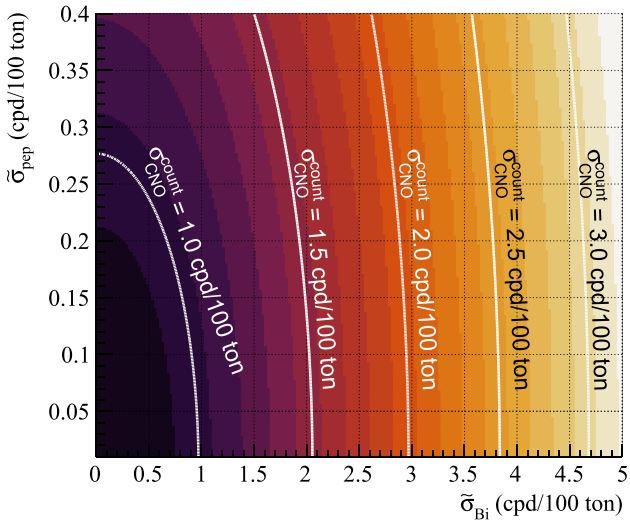

Fig. 5 The uncertainty of the CNO neutrino rate as a function of the uncertainties on *pep* neutrino and ^{210}Bi rates from the counting analysis (see Eq. (2))

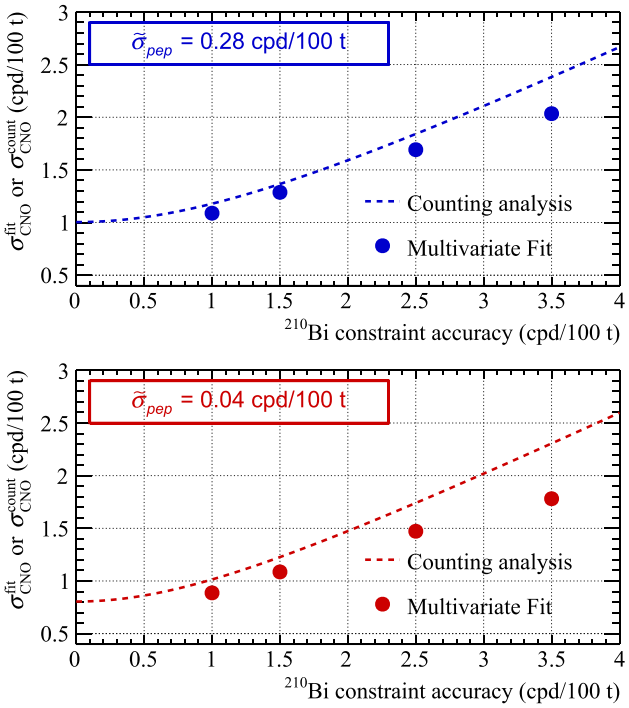

Fig. 6 Comparison between $\sigma_{\mathrm{CNO}}^{fit}$ (in solid dots) and $\sigma_{\mathrm{CNO}}^{count}$ (in dashed lines) for two values of $\tilde{\sigma}_{pep}$ and multiple $\tilde{\sigma}_{\mathrm{Bi}}$

and R_{Bi} can be independently estimated. The constraints on R_{pep} and R_{Bi} were implemented by introducing two Gaussian pull terms in the likelihood function. The centroid of the pull terms are varied according to the uncertainty of the pull. The uncertainties of the two constraints are the most important parameters when determining the sensitivity.

Each simulated dataset was fitted assuming the same detector response function as that used in the simulation. The distribution of the best-fit results for the CNO interaction rate was used to assess the expected statistical uncertainty and discovery significance. The results were obtained using the multivariate fitting tools `GooStats` [25] and `m-stats` [26].

Similarly to the data analysis of [7], the study was conducted using both Monte Carlo and analytical methods that are complementary to each other. In the Monte Carlo approach the detector response was modeled using an *ab initio* simulation software [24] that takes into account realistic and microscopic descriptions of the energy deposition, scintillation light generation and propagation, electronics response, and energy and position reconstruction. In the analytical approach, the detector response was modeled using analytical functions [19]. The analytical procedure provides an independent way of evaluating the impact of the systematic uncertainty related to detector response parameters (*e.g.*, the light yield). The two approaches gave consistent results for the expected uncertainty and discovery significance.

3.3 Uncertainty of the CNO rate

In this section the uncertainty of the CNO rate resulting from both the counting and multivariate fit analyses is discussed.

In the framework of the multivariate analysis, the distribution of the values of R_{CNO} resulting from fits performed with fixed external constraints is built. The width of this distribution is used to estimate $\sigma_{\mathrm{CNO}}^{fit}$. Figure 6 shows $\sigma_{\mathrm{CNO}}^{fit}$ as a function of the ^{210}Bi constraint uncertainty for two different values of $\tilde{\sigma}_{pep}$ as well as the uncertainty $\sigma_{\mathrm{CNO}}^{count}$ resulting from the counting analysis presented in Sect. 3.1.

In the counting analysis, the rates of ^{210}Bi and *pep* are fixed by the external constraints. Thus, according to Eq. (1), a bias on the constraints will transfer linearly to the reconstructed CNO rate. The situation becomes slightly more complicated when a full spectral analysis, combined with constraints on the background, is performed. Indeed, in the case of a bias in the external constraints, the impact on the value of the extracted CNO rate is mitigated by the tension between the shape information and the biased values.

The systematic uncertainty of the CNO rate is dominated by the bias of the ^{210}Bi accuracy (see Sect. 4.2), followed by the accuracy on the light yield.

3.4 Expected discovery significance to CNO neutrinos

A frequentist hypothesis test was performed to assess the expected discovery significance to CNO neutrinos. In the search for the CNO signal, two hypotheses are considered: the *null* hypothesis, H_0, where no CNO signal is present; and the *alternative* hypothesis, H_1, that includes the presence of

a CNO signal in addition to the background. We used the profile likelihood ratio q_0 as the test statistic [27]:

$$q_0 = -2 \ln \frac{L(H_0)}{L(H_1)}, \tag{4}$$

where $L(H_0)$ and $L(H_1)$ are the the maximum values of the likelihood against H_0 and H_1. The significance of the signal of a measurement is quantified by evaluating the compatibility of the observed data with the null hypothesis H_0 and represented by the p value. For a specific measurement with a test statistic value $q_{0,\mathrm{obs}}$, its p value is the probability that the test statistic is above $q_{0,\mathrm{obs}}$ under H_0. In quantifying the expected sensitivity of H_1 to discovery of a signal, the *median discovery significance* is used. The *median discovery significance* of H_1 is the p value of the median value of the test statistic under H_1. This requires the probability density functions (hereinafter as PDFs) of q_0 for both the null hypothesis $f(q_0|H_0)$ and the alternative hypotheses $f(q_0|H_1 = \mathrm{HZ\ or\ LZ})$.

The PDFs of the test statistics q_0 were obtained by analyzing the two sets of the simulated datasets (with and without the CNO injected), with both the simplified counting analysis and full multivariate fit. We generate 20,000 pseudo-experiments to construct the PDFs. When considering the null hypothesis, q_0 is distributed according to $1/2\delta(q_0) + \chi^2_1(q_0)$, where $\delta(q_0)$ is the Dirac-Delta function, and χ^2_1 is the PDF of the chi-square distribution with one degree of freedom. For H_1 and in the case of uncertainties of 0.04 cpd/100 ton and 1.5 cpd/100 ton on *pep* neutrinos and ^{210}Bi, respectively, the median value of the test statistic is 8.0 for HZ SSMs and 4.1 for LZ SSMs.

The expected discovery significance depends on the strength of the signal and on the precision of the external constraints: a higher rate of CNO neutrinos, as well as stronger constraints, results in a higher sensitivity. For the CNO rate predicted by the HZ SSM and in the case of uncertainties of 0.04 cpd/100 ton and 1.5 cpd/100 ton on *pep* neutrinos and ^{210}Bi, respectively, the median discovery significance to CNO neutrinos is 4.5σ. In case of the LZ SSM, it is 3.2σ. Results of the expected discovery significance under other conditions are shown in Fig. 7.

The difference between the median p value obtained from the simple counting analysis and the one from the multivariate analysis gets smaller as the precision of the constraints increase. This effect is coherent with the results on the statistical uncertainty of CNO presented in Sect. 3.3, indicating that the impact of the spectral shape information is larger when the constraints are relatively weak (high uncertainty), while it becomes negligible when the background constraints get more stringent (low uncertainty).

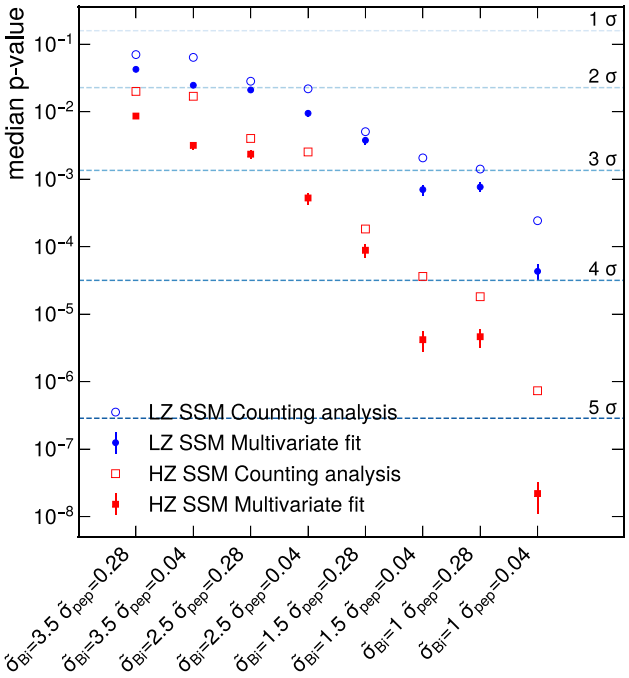

Fig. 7 Median discovery significance of a CNO neutrino signal as predicted by the HZ (in red) and LZ (in blue) SSM for different precision of the constraints on the background rates. The results of the counting analysis are indicated by empty markers and those obtained with the full multivariate fit by filled markers. The uncertainty $\tilde{\sigma}_{\mathrm{Bi}}$ and $\tilde{\sigma}_{pep}$ are in cpd/100 ton

3.5 Impact of an upper limit on ^{210}Bi rate

The method discussed in Sect. 4.2, used to obtain an independent measurement of the ^{210}Bi rate, can only provide an upper limit on the ^{210}Bi background under less stringent assumptions, that an additional contribution from migrated (diffusion and/or convection) ^{210}Po (see Sect. 4.2) is present. The presence of migrated ^{210}Po leads to a positive bias of the estimation of the ^{210}Bi rate.

In this case, the constraint is implemented in the fitting procedure as a one-sided Gaussian penalty:

$$\text{pull term} = \left(\frac{R_{\mathrm{Bi}} + R_{\mathrm{mig\ Po}} - \mu}{\sigma}\right)^2 \quad R_{\mathrm{mig\ Po}} > 0, \tag{5}$$

where $R_{\mathrm{mig\ Po}}$ is the rate of the migrated ^{210}Po as discussed in Sect. 4.2, and μ and σ are the centroid and uncertainty of the ^{210}Bi pull term. In so doing, the upper limit on the ^{210}Bi rate is equivalent to a lower limit on the CNO rate. Therefore, the expected discovery significance for CNO is the same as would be obtained using a two-sided Gaussian constraint on the ^{210}Bi rate. This was confirmed by performing a hypothesis test analogous to that described in Sect. 3.4. The results for varying widths ($\tilde{\sigma}_{\mathrm{Bi}}$) on the ^{210}Bi penalty are shown in Fig. 8. The expected discovery significance obtained from the

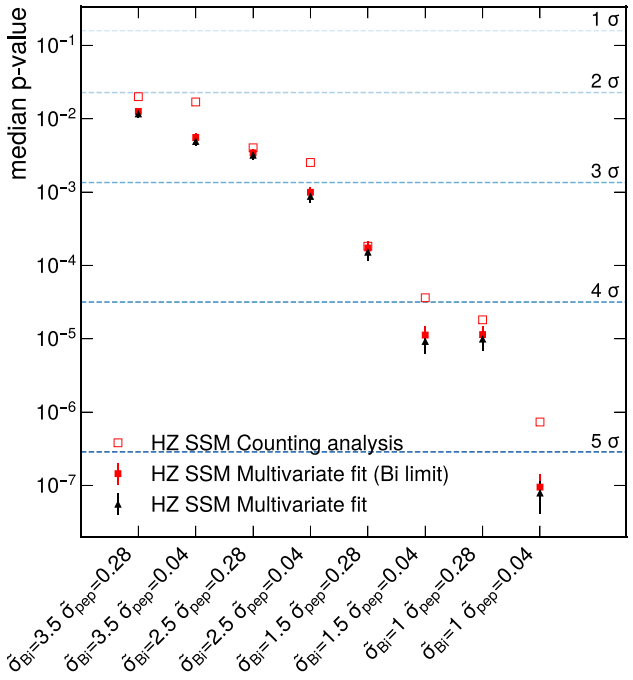

Fig. 8 Median discovery significance for the HZ hypothesis on the CNO rate when constraining the ^{210}Bi rate with an upper limit and a symmetric Gaussian penalty. The uncertainty $\tilde{\sigma}_{\rm Bi}$ and $\tilde{\sigma}_{pep}$ are in cpd/100 ton

counting analysis and from applying a symmetric constraint are also displayed for comparison. As one can see, allowing an additional contribution from the migrated ^{210}Po barely decreases the expected discovery significance for CNO.

Therefore, an upper limit on the ^{210}Bi rate may be sufficient to claim detection of CNO neutrinos, but it would not allow a precise measurement of the CNO interaction rate required to solve the solar metallicity problem. Since there is no lower limit on the ^{210}Bi rate, the upper limit of the CNO neutrino rate will not be stringent and the central CNO value might have a negative bias. Figure 9 shows the distribution of the best fit estimates, obtained from the fit of simulated datasets when applying a constraint to the *pep* neutrino rate and leaving the ^{210}Bi rate free (Fig. 9a), constraining the ^{210}Bi rate with a symmetric Gaussian penalty (Fig. 9b), and applying the upper limit described in this section (Fig. 9c).

The expected confidence intervals in Fig. 9c are asymmetric: the upper limit of the confidence interval is similar to the one obtained when leaving the ^{210}Bi rate free, while its lower limit resembles the one resulting when the ^{210}Bi rate is constrained.

4 Strategy for establishing background assessment

This section discusses the strategy for setting constraints on the *pep* neutrinos and ^{210}Bi rates independently of both the counting analysis and the multivariate fit procedure.

4.1 *pep* constraint

The electron capture reaction $p + e^- + p \rightarrow d + \nu_e$, which generates *pep* neutrinos in the Sun, is linked to the β^+ decay process $p + p \rightarrow d + e^+ + \nu_e$, which is responsible for the *pp* neutrino production, by well-known nuclear physics. Since the two processes depend on the same allowed nuclear matrix element, the ratio between their rates is determined by the available reaction phase spaces and by the electron density n_e of the solar plasma only. This ratio was calculated in [28,29], and the effect of radiative corrections subsequently discussed in [30] (see, for example, [31] for a review). It can be determined with $\sim 1\%$ precision [31] for the conditions of the solar interior and is mildly dependent on the properties of the solar plasma, roughly proportional to $T_c^{-1/2} n_e$ (where T_c is the temperature of the core of the Sun). As a consequence, the ratio $\Phi_{\rm pep}/\Phi_{\rm pp}$ between the *pep* and *pp* neutrino fluxes is a robust prediction of SSMs, and it can be used to improve the sensitivity to the CNO neutrino signal. With this approach, Borexino's direct observation of the *pp* neutrino flux [7] can be translated into a $\sim 10\%$ determination of the *pep*-neutrino component, motivating the analysis performed in Sect. 3, which assumes $\tilde{\sigma}_{pep} = 0.28$ cpd/100 ton.

The precision of the *pp* and *pep* neutrino flux determination can be further improved by performing a global analysis [32,33] on all neutrino experiment results applying the so-called solar luminosity constraint [34–36]. In this way, it was shown in [33] that the *pep* neutrino flux is constrained with $\sim 1\%$ precision of by solar neutrino data. By taking into account an additional $\sim 1\%$ uncertainty in neutrino survival probability considering the matter effects in the Sun and the uncertainty of oscillation parameters, the event rate R_{pep} can be constrained with a precision of $\sim 1.4\%$, motivating the assumption $\tilde{\sigma}_{\rm pep} = 0.04$ cpd/100 ton considered in Sect. 3. Because the contribution of CNO neutrinos to the solar luminosity is around 1%, neglecting the dependence of this *pep* constraint on the assumed $R_{\rm CNO}$ has almost no effects on the significance to CNO neutrinos, as shown in Fig. 5.

4.2 ^{210}Bi constraint

^{210}Bi is a β-emitting daughter of ^{210}Pb with a mean lifetime of 7.23 days and a Q value of 1160 keV. Since the lifetime of ^{210}Bi is small, it must be supported by its long-lasting parent nucleus ^{210}Pb ($\tau = 32.2$ years) to maintain a constant decay rate. ^{210}Pb is a part of the ^{238}U chain, and due to its low Q value of 64 keV it does not represent a background in this analysis. The ^{210}Pb and ^{210}Bi are part of the of the ^{238}U chain. The concentration of ^{238}U is estimated to be less than 9.4×10^{-20} g/g (95% C.L.) by the absence of ^{226}Ra and ^{222}Rn, easily detectable through the fast ^{214}Bi-^{214}Po coincidence following their decays in the part of the chain above

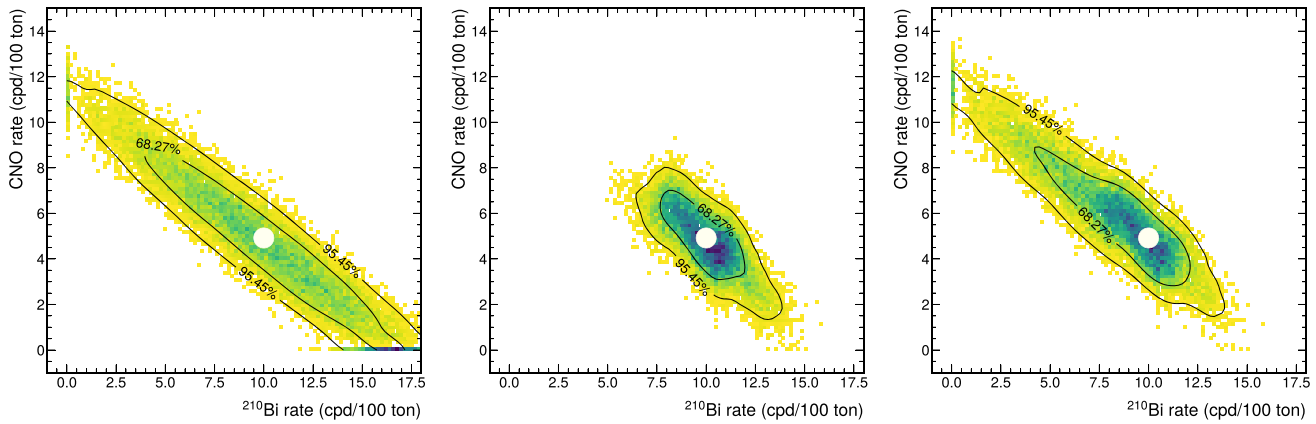

(a) free **(b)** symmetric Gaussian penalty **(c)** upper limit

Fig. 9 Distribution of the best fit results of ^{210}Bi and CNO neutrinos interaction rates obtained fitting thousands of simulated datasets applying a 10% constraint on the *pep* rate and **a** keeping ^{210}Bi free, **b** constraining ^{210}Bi with a symmetric Gaussian penalty at a precision of 1.5 cpd/100 ton, and **c** imposing an upper limit on ^{210}Bi. The injected rates of ^{210}Bi and CNO neutrinos, shown in the figures as white dots, are 10 and 4.9 cpd/100 ton, respectively

^{210}Pb. We note, that the secular equilibrium of the chain is broken at the level of ^{210}Pb. This means, that while the background from the ^{238}U chain down to ^{210}Pb is negligible, the background from the chain below ^{210}Pb is important. The purification campaign in 2011 [37], that marked the start of the Borexino Phase-II, has significantly reduced in short order the initial ^{210}Pb contamination, leading to a residual rate in the range of a few tens of cpd/100 ton.

The strategy to independently determine the ^{210}Bi rate using the decay rate of its decay product, ^{210}Po, was suggested in [8]. The isotope ^{210}Po, with a mean lifetime of 199.6 days, ends the chain by decaying into stable ^{206}Pb thereby emitting a 5305 keV α particle (visible energy around 400 keV electron equivalent):

$$^{210}\mathrm{Pb} \xrightarrow[32.2y]{\beta} {}^{210}\mathrm{Bi} \xrightarrow[7.23d]{\beta} {}^{210}\mathrm{Po} \xrightarrow[199.6d]{\alpha} {}^{206}\mathrm{Pb(stable)}.$$

When the above chain is in equilibrium, the ^{210}Bi rate is equal to that of ^{210}Po. The ^{210}Po rate can be precisely determined in Borexino because ^{210}Po emits α particles that can be identified event-by-event via pulse-shape discrimination. Using a pulse-shape analysis based on a multi-layer perceptron discriminator [21,38], ^{210}Po events in Borexino are identified with an efficiency very close to 1.

Unfortunately, the measured ^{210}Po rate is not only due to ^{210}Bi decays, but consists of three components:

1. **Unsupported ^{210}Po** The residual ^{210}Po left over by the water extraction phase of the scintillator purification campaign and not linked to local ^{210}Bi.
2. **Migrated ^{210}Po** Originally produced from the ^{210}Pb lead decays on the inner surface of the nylon vessel holding the liquid scintillator and brought into the fiducial volume by convective and diffusive motions of the liquid scintillator.
3. **Supported ^{210}Po** In secular equilibrium with local ^{210}Bi present in the liquid scintillator.

The ^{210}Bi rate is equal to the supported ^{210}Po rate and thus less than the total ^{210}Po rate in presence of the unsupported and migration terms. The rate of unsupported ^{210}Po, following the law of radioactive decay, gets asymptotically closer to zero over time with a mean lifetime of 199.6 days. The migrated ^{210}Po is the most intricate contribution to handle. In Borexino, diffusion of ^{210}Po into the fiducial volume is a completely negligible process, because on average ^{210}Po can only travel 15 cm via pure diffusion before it decays, while presence of migrated ^{210}Po is found in the center region where ^{210}Po need to travel by around 4.5 m. Therefore the movement of ^{210}Po is mainly driven by convection motion in the liquid scintillator. Because this convection motion is generated by the inhomogeneity and instability of the detector temperature, the migrated ^{210}Po is time- and space-dependent and hard to model.

These considerations are summarized through the following equation:

$$R^{\mathrm{tot}}_{\mathrm{Po}}(t) = R^{\mathrm{u}}_{\mathrm{Po}} \cdot e^{-t/\tau_{Po}} + R^{\mathrm{m}}_{\mathrm{Po}}(t) + R^{\mathrm{s}}_{\mathrm{Po}}, \tag{6}$$

where $R^{\mathrm{tot}}_{\mathrm{Po}}$ is the observed ^{210}Po rate, $R^{\mathrm{u}}_{\mathrm{Po}}$ is the initial rate of unsupported ^{210}Po decay, $R^{\mathrm{m}}_{\mathrm{Po}}$ is the migrated ^{210}Po decay rate, and $R^{\mathrm{s}}_{\mathrm{Po}}$ is the supported ^{210}Po rate and is equal to the ^{210}Bi rate.

The convective motion of the liquid scintillator was suppressed in a major effort over several years since 2015 [39]. This included the installation of a passive thermal insulation system around the water tank and an active temperature control system to mitigate seasonal modulations. Our observations showed that the migrated ^{210}Po was significantly reduced in the Borexino Phase-III which starts from 2016 June.

In Phase-III, the rate of unsupported ^{210}Po has decayed and is less than 0.1 cpd/100 ton. It is also possible to get a more precise estimate of the rate of supported ^{210}Po by identifying the region inside the fiducial volume, that is least affected by convective motions and thus with minimal migrated ^{210}Po.

The residual migrated ^{210}Po rate in this region can then be treated as a source of systematic uncertainty. Neglecting the migrated ^{210}Po rate, the statistical uncertainty of the supported term depends on the magnitude of the initial out-of-equilibrium contamination and on the exposure. As an example, with an unsupported rate of 50 cpd/100 ton and a supported rate of 10 cpd/100 ton, an precision of the order of 10% on the supported rate can be achieved in about 8 months of data-taking using the same fiducial volume of 71.3 ton as adopted in [7].

Furthermore, in order to extrapolate the value of ^{210}Bi obtained in the region with minimum ^{210}Po migration rate to the entire fiducial volume, two hypotheses must be verified: the ^{210}Bi spatial distribution must be uniform within the entire fiducial volume and its rate must follow the slow decay rate of ^{210}Pb, since there are no sources of either ^{210}Bi or ^{210}Pb in the liquid scintillator. The residual non-uniformity and instability of the ^{210}Bi rate can also be treated as systematic uncertainties of the ^{210}Bi constraint.

4.3 Impact of further scintillator purification

The purification campaign of the Borexino scintillator performed in the year 2011 [37], with 6 cycles of closed-loop water extraction, significantly reduced the concentrations of several radioactive contaminants of the scintillator. The ^{210}Bi rate was reduced by a factor ~ 2.3 [7,19]. In principle, another cycle of purification could decrease the amount of ^{210}Bi even further without introducing more ^{210}Po in the liquid scintillator. However, in order to keep the amount of migrated ^{210}Po small, thus for the sensitivity to CNO neutrinos to benefit from further purification, the thermal stability of the detector must be maintained.

In order to quantify the effect of a reduced rate of ^{210}Bi, we rewrite Eq. 2 as

$$\sigma_{\mathrm{CNO}}(R_{\mathrm{Bi}}, \mathcal{E}) = \frac{1}{\varepsilon_{\mathrm{CNO}}} \left(\sqrt{\frac{\varepsilon_{\mathrm{Bi}} R_{\mathrm{Bi}} + a_1}{\mathcal{E}}} \oplus a_2 \right), \tag{7}$$

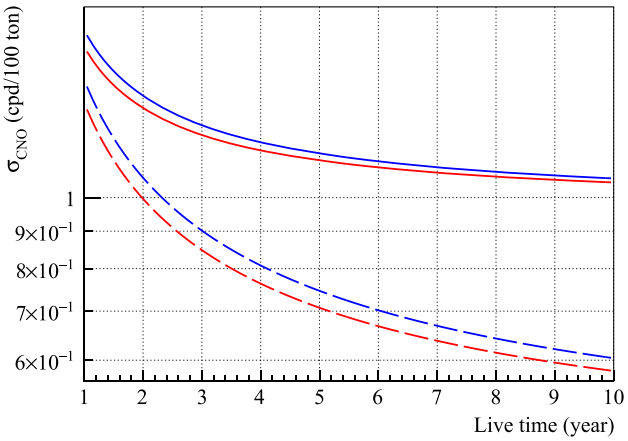

Fig. 10 Expected uncertainty on the CNO interaction rate versus live time assuming a ^{210}Bi constraint uncertainty of 1.5 (dashed line) and 0.5 (solid line) cpd/100 ton with different values of the ^{210}Bi rate. Blue line: 10 cpd/100 ton. Red line: 5 cpd/100 ton. From the figure we can see that when ^{210}Bi constraint is strong, the purification of liquid scintillator reduces the time needed to reach a given uncertainty on the interaction rate of CNO neutrinos

where $a_1 = 1.07$ cpd/100 ton is the total rate of components other than ^{210}Bi in the ROI, $a_2 = 0.06$ cpd/100 ton is the total uncertainty of the last three terms in Eq. 2 and is dominated by $\tilde{\sigma}_{\mathrm{Bi}}$, and $\mathcal{E}$ is the exposure in day$\times$ 100 ton. From Eq. 7 we see that the importance of $\mathcal{E}$ and R_{Bi} is greater when a_2 is smaller than the first term. Thus, in these conditions, reducing the rate of ^{210}Bi is equivalent to increasing the exposure. This can also be concluded from Fig. 10.

5 CNO neutrinos in the standard solar model

Despite the small contribution of the CNO cycle to the Sun's luminosity, a measurement of the CNO neutrino flux would be extremely valuable to expand our knowledge of the Sun.

Experimental measurements of solar neutrino fluxes are a fundamental test of the SSM, the benchmark of every stellar evolution model. Possible disagreements between predicted and measured neutrino fluxes may highlight issues in the model assumptions. Additionally, measurements of solar neutrino fluxes can be used to infer some properties of the Sun that are used as inputs for the SSM.

This is particularly interesting in the context of the solar metallicity problem. As mentioned in the introduction, SSMs implementing the most recent determinations of the solar surface composition (*e.g.*, the low metallicity (LZ) admixture described in [10]), fail to reproduce helioseismic observations, which agree better with models that assume a higher metal content, as prescribed by the older determinations from [14]. So far, all attempts to understand the origin of this discrepancy remain inconclusive. New experimental results on solar neutrinos could provide key pieces of information to

solve this problem. This applies in particular to the flux of CNO neutrinos, whose value differs by almost 30% between the predictions of the SSM HZ and LZ models (see Table 1).

However, the dependence of predicted solar neutrino fluxes on the metallicity and other SSM parameters is non-trivial. There is indeed a strong degeneracy between the impact of metallicity and radiative opacity through their effect on the core temperature of the Sun T_c (T_c is determined by the opacity profile, which in turn depends on the chemical composition of the solar interior). Ultimately, T_c acts as a proxy for the influence of those parameters (i.e., they impact neutrino fluxes via their effect on T_c). This degeneracy makes it difficult to disentangle metallicity from opacity with solar neutrino measurements, in particular after recent laboratory measurements [40] and theoretical advances [41–45] suggested that the uncertainty of the radiative opacity might be severely underestimated. Deviations of the radiative opacity from its nominal values can mimic the effect of a higher metal content in the Sun's core. As it was discussed in, for example, [46–48], the agreement of SSM calculations implementing the recent LZ composition and helioseismic data could be restored by considering suitable modifications to the radiative opacity. Similarly, neutrino fluxes expected by the HZ SSM can be obtained by assuming the LZ composition and a larger opacity of the solar plasma.

However, the case of the CNO neutrinos is somewhat different. In fact, the dependence of the CNO neutrino flux on metallicity is twofold: as for the other *pp*-chain neutrinos the CNO flux is indirectly linked to metallicity via T_c, but it also depends directly on the amount of carbon and nitrogen in the core of the Sun. Considering the metallicity problem, other tests of the SSM that consider measurements of ^{8}B and ^{7}Be neutrino fluxes include a larger amount of information but are greatly affected by uncertainties on the radiative opacity.

Section 5.1 shows that by exploiting this fact, a measurement of the CNO neutrino flux with Borexino can be used to infer the content of carbon and nitrogen in the Sun's core almost independently of the effect of radiative opacity, thus directly probing the solar metallicity. Section 5.2 discusses the impact of a future measurement of CNO neutrinos on the discrimination power of a hypothesis test between the HZ and LZ SSM.

5.1 CNO neutrinos as CN abundance messengers

As explained in [16], the temperature dependence for both the ^{8}B and CNO neutrino fluxes can be described by a power-law $\Phi_i \propto T_c^{\gamma_i} (i \in \{^8\mathrm{B}; \mathrm{CNO}\})$. Therefore, one can build a weighted ratio $\Phi_{\mathrm{CNO}}/(\Phi_{^8\mathrm{B}})^k$, with $k = \gamma_{\mathrm{CNO}}/\gamma_{^8\mathrm{B}}$, that is very nearly (considering different uncertainties) independent of T_c. This breaks the opacity-composition degeneracy, making it possible to infer the abundance of carbon and nitrogen in the Sun in a way that is almost independent from variations in the SSM parameters that affect the temperature profile.

To elaborate, we followed the approach of [15,16], which adopts the practice of factorizing the dependence of the neutrino flux Φ_i on the model's input parameters $\{\beta_j\}$:

$$\frac{\Phi_i}{\Phi_i^{\mathrm{SSM}}} = \prod_j^{\mathrm{sol}} x_j^{\alpha(i,j)} \cdot \prod_j^{\mathrm{met}} x_j^{\alpha(i,j)} \cdot \prod_j^{\mathrm{nucl}} x_j^{\alpha(i,j)}, \tag{8}$$

where the x_j terms are the model inputs normalised to their respective nominal SSM value (i.e., $\beta_j/\beta_j^{\mathrm{SSM}}$). These parameters are typically grouped in three categories: (*i*) the *solar* parameters, related to the Sun's astrophysical (age $A_\odot$, luminosity $L_\odot$) and non-nuclear physical properties (diffusion D, radiative opacity κ), (*ii*) the *metallicity* parameters (i.e., the abundances of C, N, O, F, Ne, Mg, Si, S, Ar, and Fe), and (*iii*) the *nuclear* cross sections of the relevant processes, described by the astrophysical S-factors. The $\alpha(i, j)$ coefficients in the exponents are normalised logarithmic partial derivatives of the fluxes with respect to the input parameters β_j

$$\alpha(i, j) = \frac{\mathrm{d}\ln(\Phi_i/\Phi_i^{\mathrm{SSM}})}{\mathrm{d}\ln(\beta_j/\beta_j^{\mathrm{SSM}})}, \tag{9}$$

which are typically provided along with SSM predictions.

Using Eq. 8 to express solar neutrino fluxes, the aforementioned weighted ratio between the ^{15}O and ^{8}B fluxes reads:

$$\left(\frac{\Phi_{^{15}\mathrm{O}}}{\Phi_{^{15}\mathrm{O}}^{\mathrm{SSM}}}\right) \Big/ \left(\frac{\Phi_{^8\mathrm{B}}}{\Phi_{^8\mathrm{B}}^{\mathrm{SSM}}}\right)^k = \prod_j x_j^{\alpha(^{15}\mathrm{O},j) - k\alpha(^8\mathrm{B},j)}. \tag{10}$$

To reduce the dependence on T_c, the weight k is chosen such that it minimizes the uncertainty of the quantity defined in Eq. 10 due to the so-called *environmental* parameters (i.e., those SSM inputs which affect the Sun's temperature profile the most [15,16]). These parameters include the *solar* and *metallicity* parameters discussed above, but without the C and N abundances.

When applying this strategy to Borexino we refer, for simplicity, to the counting analysis described in Sect. 3.1. In this narrow energy window, neglecting insignificant ^{17}F neutrinos, CNO neutrino events originate from contributions of ^{15}O and ^{13}N neutrinos. We thus define the flux of CNO neutrinos measured by Borexino $\Phi_{\mathrm{CNO}}^{\mathrm{BX}}$ as a combination of $\Phi_{^{15}\mathrm{O}}$ and $\Phi_{^{13}\mathrm{N}}$. This can be written as:

$$\frac{\Phi_{\mathrm{CNO}}^{\mathrm{BX}}}{\Phi_{\mathrm{CNO}}^{\mathrm{SSM}}} = \xi \frac{\Phi_{^{15}\mathrm{O}}}{\Phi_{^{15}\mathrm{O}}^{\mathrm{SSM}}} + (1-\xi) \frac{\Phi_{^{13}\mathrm{N}}}{\Phi_{^{13}\mathrm{N}}^{\mathrm{SSM}}}, \tag{11}$$

where ξ is the ratio between the event rate of ^{15}O neutrinos and all CNO neutrinos in the ROI, as expected from the SSM:

$$\xi \equiv r^{\rm SSM}_{^{15}\rm O} / \left(r^{\rm SSM}_{^{15}\rm O} + r^{\rm SSM}_{^{13}\rm N} \right) = r^{\rm SSM}_{^{15}\rm O} / r^{\rm SSM}_{\rm CNO} = 0.764. \quad (12)$$

Using the logarithmic derivatives of ^{15}O and ^{13}N neutrinos from the B16-SSM [6], we can describe the dependence of the measured CNO neutrino flux on the inputs of the SSM as

$$\alpha(\rm CNO^{BX}, \mathit{j}) = \xi\, \alpha(^{15}\rm O, \mathit{j}) + (1-\xi)\, \alpha(^{13}\rm N, \mathit{j}). \quad (13)$$

Having computed those derivatives, we can express Eq. 10 using a CNO measurement by Borexino and the ^{8}B neutrino flux measured by Super-Kamiokande [17]. In the case of Borexino, the value of k, obtained from a minimization of the uncertainty from the *environmental* parameters, is found to be 0.716. To explicitly show the dependence on all SSM inputs:

$$\begin{aligned} &\frac{\Phi^{\rm BX}_{\rm CNO}}{\Phi^{\rm SSM}_{\rm CNO}} \Big/ \left[\frac{\Phi_{^8\rm B}}{\Phi^{\rm SSM}_{^8\rm B}} \right]^{0.716} = x_{\rm C}^{0.814}\, x_{\rm N}^{0.191}\, x_{D}^{0.184} \\ &\times \left[x_{L_\odot}^{0.618}\, x_{\kappa_a}^{0.023}\, x_{\kappa_b}^{-0.048}\, x_{A_\odot}^{0.274} \right] \\ &\times \left[x_{\rm O}^{0.005}\, x_{\rm Ne}^{-0.004}\, x_{\rm Mg}^{-0.003}\, x_{\rm Si}^{0.001}\, x_{\rm S}^{0.001}\, x_{\rm Ar}^{0.001}\, x_{\rm Fe}^{0.004} \right] \\ &\times \left[x_{S_{11}}^{-0.820}\, x_{S_{33}}^{0.324}\, x_{S_{34}}^{-0.647}\, x_{S_{e7}}^{0.715}\, x_{S_{17}}^{-0.736}\, x_{S_{114}}^{0.978} \right], \end{aligned} \quad (14)$$

where the contributions of the environmental parameters[1] are grouped in the second and third rows on the right-hand side, while the contributions of nuclear cross sections are in the fourth row. Following [15,16], the exponents in Eq. 14 were obtained using the values of the logarithmic derivatives of the solar neutrino fluxes with respect to the SSM inputs used by the HZ SSM [6].

Assuming, for simplicity, that the C and N abundances are modified by the same factor (i.e., $x_{\rm C} = x_{\rm N} \equiv (N_{\rm C} + N_{\rm N})/(N^{\rm SSM}_{\rm C} + N^{\rm SSM}_{\rm N})$, where $N_{\rm C}$ and $N_{\rm N}$ indicate the number density of C and N with respect to hydrogen) and noticing in Eq. 14 that the sum of the exponents of $x_{\rm C}$ and $x_{\rm N}$ is $0.814 + 0.191 \simeq 1$, we can invert the formula, obtaining:

$$\begin{aligned} \frac{N_{\rm C} + N_{\rm N}}{N^{\rm SSM}_{\rm C} + N^{\rm SSM}_{\rm N}} = &\left(\frac{\Phi_{^8\rm B}}{\Phi^{\rm SSM}_{^8\rm B}} \right)^{-0.716} \\ &\times \frac{R^{\rm BX}_{\rm CNO}}{R^{\rm SSM}_{\rm CNO}} \times [1 \pm 0.5\%(\rm env) \\ &\pm 9.1\%(\rm nucl) \pm 2.8\%(\rm diff)], \end{aligned} \quad (15)$$

[1] The radiative opacity is represented by two parameters, namely $\kappa_a \equiv 1 + a$ and $\kappa_b \equiv 1 + b$, which describe the variations of the solar opacity profile in terms of the parameters a and b defined in [6].

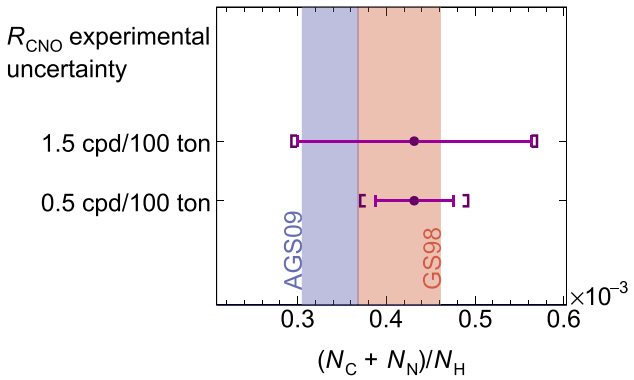

Fig. 11 Projected uncertainty in the determination of the (C+N) abundance from a measurement of CNO neutrinos under different precision scenarios. The error bars indicate the error budget due to the experimental precision in the measurement of CNO solar neutrinos, while the overall uncertainty – accounting for the limited precision of the SSM inputs and for the ^{8}B solar neutrino uncertainty – is enclosed in square brackets. These results have been obtained assuming the rate expected from the HZ SSM and using the result of [33] for the ^{8}B flux. The red and blue bands show the 68% confidence interval of the abundance of carbon and nitrogen reported in the GS98 [14] and in the AGS09 [10] catalogues respectively

where $R^{\rm BX}_{\rm CNO}$ is the rate measured by Borexino and proportional to the flux $\Phi^{\rm BX}_{\rm CNO}$. The quoted uncertainties were obtained by propagating the uncertainties of the environmental, nuclear, and diffusion parameters used in the SSM. The current uncertainty on the measurement of the boron neutrino flux is about 2% [33]. The dominant contributions to the uncertainty budget besides the CNO neutrino rate are from nuclear reactions, with the largest coming from S_{114} (7.3%), S_{34} (3.4%), and S_{17} (3.5%).

The low level of the environmental contribution to the total error budget (which takes into account all SSM parameters except nuclear reactions and diffusion coefficients) demonstrates that a future CN flux measurement will be converted into an almost direct determination of the C+N content of the solar core, as discussed in [15,16].

The impact of the experimental and model uncertainties in the determination of the C+N abundance inferred from a CNO neutrino measurement, assuming the rate predicted by the HZ SSM, is represented in Fig. 11. While a 1.5 cpd/100 ton precision is translated, according to Eq. 15, to a precision that is about three to four times larger than the precision of the GS98 and AGSS09 catalogues, a future measurement of $R_{\rm CNO}$ with a precision $\simeq 0.5$ cpd/100 ton (achievable by next generation experiments [49–51]) will be able to constrain the C+N fraction of the Sun with an uncertainty $\simeq 15\%$, which is comparable to the precision of the current estimations obtained from measurements of the photosphere.

5.2 High versus low metallicity standard solar model

If one considers the current treatment of the opacity and of its corresponding uncertainties in the SSM as reliable, then the measurements of neutrino fluxes due to the *pp* chain can also be used to test models of the composition of the Sun.

In the results of Borexino Phase-II [7], the measurement of the fluxes of ^{7}Be and ^{8}B neutrinos were used to this end because of their strong dependence on the Sun's core temperature, which is affected by the metal content as described above. Including CNO neutrinos in a similar test is particularly interesting since their flux depends on the carbon and nitrogen abundances in the Sun. This strong dependence on the SSM parameters leads to a 30% difference between the predictions of the CNO neutrino flux of the HZ and LZ SSMs (See Table 1).

In order to assess the relevance of a future CNO flux determination in this context, we performed a frequentist hypothesis test analogue to the one described in [7] and considered the HZ and LZ SSMs as the alternative hypothesis (H_1) and the null hypothesis (H_0), respectively. Namely, we assumed a given model and determined the p value against the alternative hypothesis when the ^{8}B, ^{7}Be, and CNO neutrino rates were measured with prescribed accuracies. For ^{8}B and ^{7}Be neutrinos, we adopted the rate uncertainties from [7]. This makes it possible to directly compare our results with the one from [7] that did not incorporate CNO neutrinos in the analysis. To simulate future CNO neutrino measurements, we used uncertainties of 1.5 and 0.5 cpd/100 ton, as discussed in the previous sections.

Our results are shown in Fig. 12, where we plot the distributions of the test statistic defined as the difference between the χ^2 computed for HZ and LZ predictions including both model and experimental uncertainties. The more the distributions are separated, the higher the probability of discriminating among the different hypotheses is.

When taking into account values for the ^{8}B and ^{7}Be neutrino fluxes as predicted by the HZ SSM and measured with the same precision as in [7], the median p value for the LZ predictions is 0.057, corresponding to a 1.6σ significance in the exclusion of the wrong hypothesis. When including a measurement of CNO neutrinos with an uncertainty of 1.5 cpd/100 ton, the median discriminatory power for the LZ SSM hypothesis does not change significantly (p value $= 0.047$, 1.7σ significance), as the experimental uncertainty is 2–3 times larger than the model precision. A larger increase in significance can be obtained if a 0.5 cpd/100 ton precision in the determination of the CNO neutrino flux is achieved. In this case, assuming the HZ SSM predictions, the median p value for the LZ SSM is 0.016 (2.1σ). Similar significance levels were found when using the values of $\Phi_{^{8}\mathrm{B}}$ and $\Phi_{^{7}\mathrm{Be}}$ measured by Borexino in [7].

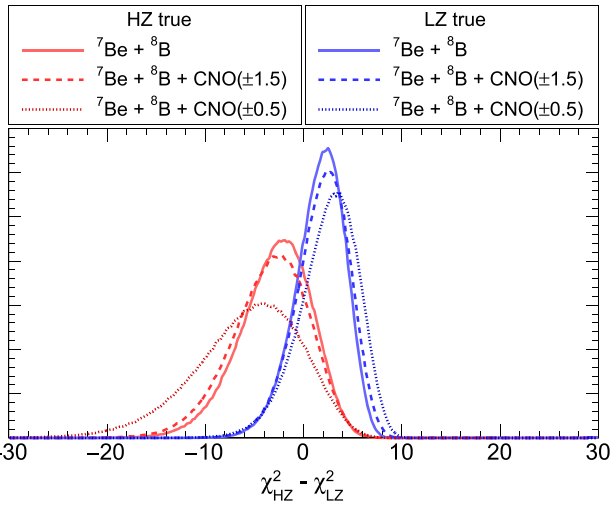

Fig. 12 PDFs of a test statistics suited to perform a hypothesis test between the HZ and LZ SSM. The solid-line PDFs indicates the expected distributions obtained considering only ^{8}B and ^{7}Be neutrinos obtained with the same precision as reported by Borexino in [7], while the distributions with dashed and dotted lines are obtained including in the analysis a future measurement of CNO neutrinos with an precision of 1.5 and 0.5 cpd/100 ton, respectively

This test relies on stronger assumptions as the determination of C+N abundance presented in the previous section. It also considers a simplified "binary" hypothesis system where either the HZ and LZ SSM is assumed to be correct, with no possible alternative explanation. However, its discriminatory power is better than the one achievable from the inferred C+N abundance for the simple reason that while in the latter the impact of metallicity on the core temperature is cancelled out, in this study it is the dominant source of information, driving the sensitivity of the test through $\Phi_{^{8}\mathrm{B}}$ and $\Phi_{^{7}\mathrm{Be}}$. In this context, a measurement of CNO neutrinos is expected to have a sensible impact on the test only if the experimental precision approaches model uncertainty (i.e., $\sigma_{\mathrm{CNO}} \simeq 0.5$ cpd/100 ton). The precision of the solar model predictions indeed poses a strong limit to the overall sensitivity of such a test. Currently, the largest sources of uncertainty – besides the plasma opacity and the carbon abundance – are the S_{17} (^{8}B), S_{34} (^{7}Be), and S_{114} (CNO) astrophysical S-factors [6]. Therefore, a reduction of the nuclear cross section uncertainties is crucial to allow for a more significant test of the SSM based on solar neutrino measurements.

6 Conclusions

Borexino has a a strong potential to detect CNO neutrinos due to its unique radiopurity, intrinsically low cosmogenic ^{11}C rate and successful TFC method for its further reduction, reduction of external gammas by passive detector shielding, as well as comprehensive detector and background modeling.

A detailed sensitivity study was performed which showed that if the backgrounds are constrained, the bulk of the sensitivity to the CNO neutrino signal can be established with a simple counting analysis. The multivariate analysis only mildly improves this sensitivity when the uncertainty on the background rates is relatively loose. The statistical uncertainty on the CNO rate depends on the uncertainty in the determination of the *pep* neutrinos and ^{210}Bi backgrounds. If R_{Bi} and R_{pep} can be constrained with a 1.5 cpd/100 ton and 0.04 cpd/100 ton precision, respectively, the expected uncertainty of CNO neutrino rate is 1.2 cpd/100 ton, and the expected median discovery significance to CNO neutrinos is 4.1σ (3.0σ) for the CNO flux assuming the HZ (LZ) SSM.

The sensitivity does not improve significantly if a new purification campaign were to further reduce the ^{210}Bi content, unless the absolute precision of the ^{210}Bi constraint is improved. This improvement is not guaranteed by the reduction of the ^{210}Bi content alone and is mainly related to the capability of stabilizing the detector temperature and suppressing convective motions. However, for a given uncertainty on the ^{210}Bi constraint and if the uncertainty on the rate of CNO neutrinos is dominated by statistical fluctuations, a reduction of ^{210}Bi would shorten the time needed to achieve a given precision on the CNO neutrino interaction rate.

In order to break the correlations, the *pep* and ^{210}Bi background rates must be independently constrained. The rate of *pep* neutrinos can be constrained by exploiting its relation with the *pp* neutrino rate as already done in the analysis presented in [7]. The uncertainty on the *pep* rate can be reduced to the level of around one percent by imposing an additional constraint based on solar luminosity measurements.

The ^{210}Bi isotope is supported by their long-lived parent ^{210}Pb ($\tau_{\mathrm{Pb}} = 32.2$ years). The most promising method to constrain the ^{210}Bi background relies on a measurement of the daughter isotope ^{210}Po, which is expected to be in equilibrium with the ^{210}Pb when the liquid scintillator is thermally stable. ^{210}Po events can efficiently be tagged using pulse-shape discrimination. Since mid-2015, the Borexino collaboration has been focusing its effort on the thermally stabilizing the detector.

By combing the measurements of $\Phi_{^8\mathrm{B}}$ and Φ_{CNO}, the carbon and nitrogen contents of the solar core can be determined independently of the opacity of solar plasma. Assuming R_{CNO} is measured with an uncertainty $\simeq 0.5$ cpd/100 ton, the C+N fraction of the Sun can be determined within $\simeq 15\%$, which is comparable to the precision of the current estimations obtained from measurements of the photosphere, and limited by the nuclear cross section precision.

The neutrino fluxes depend on the chemical composition of the Sun, and can be used to discriminate between SSM HZ and LZ models. Combining the measurements of $\Phi_{^7\mathrm{Be}}$, $\Phi_{^8\mathrm{B}}$, and Φ_{CNO}, assuming the CNO rate to be determined at a precision of 0.5 cpd/100 ton, the median discrimination sensitivity is 2.1σ and limited by the uncertainties of SSM.

Acknowledgements The Borexino program is made possible by funding from Istituto Nazionale di Fisica Nucleare (INFN) (Italy), National Science Foundation (NSF) (USA), Deutsche Forschungsgemeinschaft (DFG) and Helmholtz-Gemeinschaft (HGF) (Germany), Russian Foundation for Basic Research (RFBR) (Grants No. 16-29-13014ofi-m, No. 17-02-00305A, and No. 19-02-00097A) and Russian Science Foundation (RSF) (Grant No. 17-12-01009) (Russia), and Narodowe Centrum Nauki (NCN) (Grant No. UMO 2017/26/M/ST2/00915) (Poland). We gratefully acknowledge the computing services of Bologna INFN-CNAF data centre and U-Lite Computing Center and Network Service at LNGS (Italy), and the computing time granted through JARA on the supercomputer JURECA [52] at Forschungszentrum Jülich (Germany). This research was supported in part by PLGrid Infrastructure. We acknowledge also the generous hospitality and support of the Laboratori Nazionali del Gran Sasso (Italy).

Data Availability Statement This manuscript has associated data in a data repository. [Authors' comment: The datasets generated during the current study are freely available in the repository https://bxopen.lngs.infn.it/. Additional information is available from the Borexino Collaboration spokesperson (spokesperson-borex@lngs.infn.it) upon reasonable request.]

Funded by SCOAP[3].

References

1. D. Clayton, *Principles of stellar evolution and nucleosynthesis* (University of Chicago Press, Chicago, 1983)
2. J. Bahcall, *Neutrino astrophysics* (Cambridge University Press, Cambridge, 1989)
3. M. Salaris, S. Cassisi, *Evolution of stars and stellar populations* (Wiley, New York, 2005)
4. R. Kippenhahn, A. Weigert, A. Weiss, *Stellar structure and evolution* (Springer, New York, 2012)
5. S. Degl'Innocenti, G. Fiorentini, B. Ricci, F. Villante, Phys. Lett. B **590**(1), 13–20 (2004)
6. N. Vinyoles et al., Astrophys. J. **835**(2), 202 (2017)
7. M. Agostini et al. (Borexino Coll.), Nature **562**, 505–510 (2018)
8. F. Villante et al., Phys. Lett. B **701**(3), 336–341 (2011)
9. M. Asplund, N. Grevesse, A. Sauval, Nucl. Phys. A **777**, 1–4 (2006) **(special issue on Nuclear Astrophysics)**
10. M. Asplund, A. Grevesse, N. Sauval, P. Scott, Annu. Rev. Astron. Astrophys. **47**(1), 481–522 (2009)
11. P. Scott et al., Astron. Astrophys. **573**(A25), 1–19 (2015)

12. P. Scott, M. Asplund, N. Grevesse, M. Bergemann, A. Sauval, Astron. Astrophys. **573**(A26), 1–33 (2015)
13. E. Caffau, H.-G. Ludwig, M. Steffen, B. Freytag, P. Bonifacio, Sol. Phys. **268**(2), 255–269 (2011)
14. N. Grevesse, A. Sauval, Space Sci. Rev. **85**(1), 161–174 (1998)
15. A. Serenelli, C. Peña Garay, W.C. Haxton, Phys. Rev. D **87**, 1–9 (2013)
16. W.C. Haxton, A.M. Serenelli, Astrophys. J. **687**(1), 678–691 (2008)
17. K. Abe et al. (Super-Kamiokande Coll.), Phys. Rev. D **94**(5), 052010 (2016)
18. G. Bellini et al. (Borexino Coll.), Phys. Rev. D **89**(11), 1–68 (2014)
19. M. Agostini, Zenodo (2020). https://doi.org/10.5281/zenodo.4209228
20. G. Alimonti et al. (Borexino Coll.), Nucl. Instrum. Methods A **600**, 3, 568–593 (2009)
21. M. Agostini et al. (Borexino Coll.), Astropar. Phys. **92**, 21–29 (2017)
22. M. Agostini et al. (Borexino Coll.), Phys. Rev. D **101**(1), 12009 (2020)
23. I. Esteban et al., J. High Energy Phys. **2017**(1), 87 (2017)
24. M. Agostini et al. (Borexino Coll.), Astropar. Phys. **97**, 136–159 (2018)
25. X. Ding, J. Instrum. **13**(12), P12018–P12018 (2018)
26. M. Agostini, M-STATS: framework for frequentist statistical analysis (2016). https://github.com/mmatteo/m-stats
27. G. Cowan, K. Cranmer, E. Gross, O. Vitells, Eur. Phys. J. C **71**(2), 1–19 (2011)
28. J. Bahcall, R. May, Astrophys. J. **155**, 501 (1969)
29. J. Bahcall, Phys. Rev. D **41**, 2964–2966 (1990)
30. A. Kurylov, M. Ramsey-Musolf, P. Vogel, Phys. Rev. C **67**, 12 (2003)
31. E.G. Adelberger et al., Rev. Mod. Phys. **83**, 195–245 (2011)
32. F. Capozzi, E. Lisi, A. Marrone, A. Palazzo, J. Phys. Conf. Ser. **1312**, 012005 (2019). https://doi.org/10.1088/1742-6596/1312/1/012005
33. J. Bergström et al., J. High Energy Phys. **2016**, 132 (2016)
34. J. Bahcall, Phys. Rev. C **65**, 5 (2002)
35. V. Castellani, S. Degl'Innocenti, G. Fiorentini, M. Lissia, B. Ricci, Phys. Rept. **281**, 309–398 (1997)
36. F. Vissani, in ed. by M. Meyer, K. Zuber (eds.) *Solar Neutrinos* (2019), pp. 121–141. arXiv:1808.01495
37. A. Ianni, Acta Phys. Pol., A **121**(1), 101–103 (2012)
38. M. Agostini et al. (Borexino Coll.) (2020)
39. W.A. Bravo-Berguño et al., Nucl. Instrum. Methods Phys. Res. Sect. A **885**, 38–53 (2018). https://doi.org/10.1088/1742-6596/1312/1/012005
40. J. E. Bailey et al., Nature **517**(7532), 56–59 (2015)
41. M. Krief, Y. Kurzweil, A. Feigel, D. Gazit, Astrophys. J **856**(2), 135 (2018)
42. J. Colgan et al., Astrophys. J **817**(2), 116 (2016)
43. C.A. Iglesias, Mon. Not. R. Astron. Soc. **450**(1), 2–9 (2015)
44. M. Krief, A. Feigel, D. Gazit, Astrophys. J **821**(1), 45 (2016)
45. C. Blancard, P. Cossé, G. Faussurier, Astrophys. J **745**(1), 1 (2012)
46. J. Bahcall, S. Basu, M. Pinsonneault, A. Serenelli, Astrophys. J. **618**, 623–626 (2005)
47. J. Christensen-Dalsgaard, M. Di Mauro, G. Houdek, F. Pijpers, Astron. Astrophys. **494**(1), 205–208 (2009)
48. F. Villante, Astrophys. J. **724**, 623–626 (2010)
49. D. Franco et al., J. Cosmol. Astropart. P. **2016**, 8 (2016). arXiv:1510.04196
50. M. Askins, Z. Bagdasarian, N. Barros et al., THEIA: an advanced optical neutrino detector. Eur. Phys. J. C **80**, 416 (2020). https://doi.org/10.1140/epjc/s10052-020-7977-8
51. J.F. Beacom et al., Chin. Phys. C **41**, 2 (2017)
52. Jülich Supercomputing Centre, J. Large Scale Res. Facilities **4**, A132 (2018)